Peer-reviewed version available at Int. J. Mol. Sci. 2019, 20, 2709; doi:10.3390/ijms20112709

Article

Enhanced protection of biological membranes during lipid peroxidation. Study of the interactions between flavonoid loaded mesoporous silica nanoparticles and model cell membranes.

Anja Sadžak [1], Lucija Mandić [1], Vida Strasser [1], Goran Baranović [2], Darija Domazet Jurašin [1], Maja Dutour Sikirić [1] and Suzana Šegota [2,*]

[1] Ruđer Bošković Institute, Division of Physical Chemistry, 10000 Zagreb, Croatia 1; e-mail@e-mail.com
[2] Ruđer Bošković Institute, Division of Organic Chemistry and Biochemistry, 10000 Zagreb, Croatia
* Correspondence: ssegota@irb.hr; Tel.: ++385-1- 456-1185

Abstract: Flavonoids, polyphenols with anti-oxidative activity have high potential as novel therapeutics for neurodegenerative disease, but their applicability is rendered by their poor water solubility and chemical instability under physiological conditions. In this study, this is overcome by delivering flavonoids to model cell membranes (unsaturated DOPC) using prepared and characterized biodegradable mesoporous silica nanoparticles, MSNs. Quercetin, myricetin and myricitrin have been investigated in order to determine the relationship between flavonoid structure and protective activity towards oxidative stress i.e. lipid peroxidation induced by addition of hydrogen peroxide and/or Cu^{2+} ions. Among investigated flavonoids, quercetin showed the most enhanced and prolonged protective anti-oxidative activity. The nanomechanical (Young modulus) measurement of the MSNs treated DOPC membranes during lipid peroxidation confirmed attenuated membrane damage. By applying combination of experimental techniques (AFM, force spectroscopy, ELS, DLS), this work generated detailed knowledge about the effects of flavonoid loaded MSNs on the elasticity of model membranes, especially under oxidative stress conditions. Results from this study will pave the way towards the development of innovative and improved markers for oxidative stress-associated neurological disorders. In addition, the obtained could be extended to designing effective delivery systems of other high potential bioactive molecules with an aim to improve human health in general.

Keywords: lipid peroxidation; membrane elasticity; mesoporous silica nanoparticles; myricetin; myricitrin; nanomechanics; protective effects of flavonoids; quercetin

1. Introduction

Oxidative stress is one of the major causes of neuronal death in a variety of neurodegenerative diseases [1]. It occurs when cellular antioxidant defense is insufficient to keep the levels of reactive oxygen species (ROS) below a toxic threshold. Antioxidant defense engaged in maintenance of redox homeostasis is provided by various biological antioxidants such as reduced glutathione (GSH) and by diverse antioxidant enzymes. Among different biological molecules, polyunsaturated fatty acids (PUFAs) abundant in neuronal membranes are highly prone to ROS-induced lipid peroxidation, a chain reaction of free radical formation in the lipid parts of cellular membranes. This is particularly important in relation to the brain, because the brain is highly vulnerable to oxidative damage [2,3]. It

is considered that a decrease of ROS generated by antioxidants could be an effective therapeutic strategy in neuroprotection. High potential of the flavonoids to regain redox homeostasis and prevent or delay neuronal oxidative injury is strongly emphasized in recent years [4].

Flavonoids are a broad class of polyphenolic biomolecules, with numerous hydroxyl groups, found in a variety of fruits and vegetables. They exert different biological activities such as, anticarcinogenic [5], antiinflammatory [6] and antibacterial activity [7]. Presumably they possess remarkable therapeutic potential in preventing the onset and progression of Alzheimer's disease and in promoting cognitive performance [8]. They might facilitate a protective or preventive effect in model systems for studying Alzheimer's disease [9]. However, the mechanisms involved in antioxidant effects of flavonoids have not yet been fully elucidated. In addition, the use of flavonoids has been limited due to their poor water solubility, i.e. high hydrophobicity, and chemical instability under physiological conditions [10].

A promising way to deliver poorly soluble bioactive molecules is their incorporation within nanoparticles (NPs) [11-13]. Among different NPs, biodegradable NPs are gaining increased attention for their ability to serve as a viable nanocarriers for site specific delivery of biomolecules in the body and offer enhanced biocompatibility and convenient release profiles for a number of drugs, vaccines and biomolecules [14]. Up to now for flavonoid delivery, different organic (liposomes, dendrimers, polymer NPs and lipid NPs [15, 16]) and inorganic (gold NPs, TiO_2 NPs, Fe_3O_4 [17-19]) NPs were used. Lately biodegradable mesoporous MNPs emerge as the ones having ideal properties for designing nano-particulate delivery system: effectively controlled particle size and surface chemistry; enhanced permeation, flexibility, solubility and release of therapeutically active agents in order to attain the target and specific activity at a predetermined rate and time [20, 21]. Due to their large active surface area and high pore volume, they are able to host diverse molecules and as result have the highest drug-loading efficiency [13, 20, 22]. In addition, they can provide excellent physico-chemical protection from their degradation in physiological conditions, like during endogenic enzymatic activities [12, 20]. Mesoporous silica nanoparticles (MSNs) presents promising flavonoids nanocarriers. They have high loading efficacy, sustained release properties and subcellular size which makes them promising drug delivery carrier systems. The reproducible protocol for biodegradable mesoporous silica NPs production is well established [11, 23, 24]. They are widely used for the controlled delivery of drugs and proteins [11, 12, 20 , 25]. In order to confirm usefulness of this approach, we will also investigate interactions between MSNs and membranes since they are crucially important both for the cell uptake and nanotoxicity [26]. By using mesoporous nanoparticles MSNS, we achieved three goals: (i) to increase the flavonoid loading, as compared to so far used organic or inorganic NPs; (ii) to protect flavonoids from chemical degradation under physiological conditions and (iii) to enable sustained flavonoid release due to MSNs mesoporous structure. Within this study, flavonoids from the subgroups of flavonols, quercetin [27, 28], myricetin [29] and myricitrin [30] have been investigated. Such choice of flavonoids enables determination of a relationship between flavonoid structure and protective activity towards oxidative stress. All selected flavonoids contain planar moiety but differ in the degree of monosaccharide unit substitution. Literature data show that upon therapeutic intervention with quercetin, significant neuroprotection as well as neuronal recovery can be achieved [27, 28]. Myricetin is a natural flavonol from fruits, vegetables, tea, berries, red wine and medical plants. Myricetin exhibits antioxidative, anticancerogenic and antiinflammatory effects with strong scavenging activity [29] and is able to protect a variety of cells from in vitro and in vivo injury [6, 29, 31]. However, the antioxidant ability of myricetin in vitro is less apparent in vivo due in part to a low solubility and relatively poor bioavailability [20]. Myricitrin reportedly possesses effective antioxidative effect with strong free radical scavenging activity [30]. Moreover, the antiinflammatory potential [32], antinociceptive effect [Meotti, 2006 , enzyme inhibitory effect [Sun, 2013 and neuroprotective action [33] findings suggest that myricitrin exhibits a significant heteroprotective role.

Key step for resolving this difficulty is determining the biophysical behavior of lipid membranes as characterized, for example by permeability, elasticity and/or fluidity upon exposure to MSNs [14].

Furthermore, this behavior was shown to be influenced by the chemical composition of the surrounding solvent, MSNs surface functionality [34, 35] and release kinetics of flavonoids from the MSNs. Besides, released from MSNs, flavonoids are capable to penetrate deep more or less into the hydrophobic or interphase sites of biological membranes, particularly compartments known as lipid rafts, depending on the flavonoid hydrophilicity and/or hydrophobicity. Consequently, membrane hosted flavonoids influence on the biophysical (membrane microviscosity, transmembrane potential) [36, 3], thermotropic (phase transition temperature) [38, 39] and nanomechanical properties (elasticity e.g. fluidity, permeability) [40] of the cell membrane by controlling the arrangement of membrane constituents responsible for cell signal transduction, the regulation of the metabolism and biological activity [41].

The complex cell membrane structure along with highly dynamic membrane processes, particularly interactions with drugs and drug delivery systems, are very difficult to investigate from the biophysical point of view. Therefore, simplified membrane model systems (liposomes, supported lipid bilayers (SLBs), lipid monolayers) have been developed that are the subject of numerous long-term researches. In all the studies, as the model membrane system, phospholipids were, particularly unsaturated dioleoyl-phosphatdylcholine (DOPC) [42]. The advantage of the using such model lipid membranes without other membrane components lies in their avoiding of the interference that enables the focus on the process of their mutual interaction with lipid membranes. These interactions are essentially responsible for the development of novel drugs and at least enabled the deep insight of their therapeutic potentials.

Many of techniques were applied for the studies of very broad spectra of flavonoids and flavonoid induced changes in membrane fluidity, but it should be very careful using direct comparison of reported results [43]. In number of recent studies have been reported that, depending on the used lipid, flavonoid, and surrounding media, the mode of action is only partially understood. Besides functional proteins (enzymes) flavonoids react with lipid bilayers and influence membrane properties. The hydrophilic flavonoids form the hydrogen bonds between flavonoid molecules and the polar membrane interface [44] inducing the membrane rigidification or decrease of fluidity. On the other hand, the more hydrophobic flavonoids showed marked affinity for the membrane interior and therefore caused significant membrane permeability. Consequently, both polar and nonpolar forces were shown to have a significant impact on the flavonoid-membrane interactions [45]. Induced rigidification effect is presumed to hamper the radical diffusion and decreases the kinetics of radical reactions within membrane environment, resulting in the inhibition of lipid peroxidation process [46]. However, the modification (increase or decrease) of membrane fluidity is undoubtedly responsible for the antioxidative effects of flavonoids, or drugs, in general.

The innovation provided by this study is the measurement of the membrane structural reorganization induced by peroxidation/copper ions by combining AFM imaging as well as non-imaging data. Among investigated flavonoids, quercetin, incorporated in MSNs showed the most enhanced and prolonged protective anti-oxidative activity. The nanomechanical (Young modulus) measurement of the MSNs treated DOPC membranes during lipid peroxidation confirmed attenuated lipid peroxidation. By applying combination of experimental techniques that are not fully exploited until now in the field of molecular biotechnology (atomic force microscopy (AFM), force spectroscopy (FS and dynamic/electroforetic light scattering (DLS/ELS)), this study ultimately generated detailed knowledge about the effects of the structure and hydrophobicity of flavonoids loaded in MSNs on model lipid membranes under conditions of oxidative stress. Specific information about how the structural and nanomechanical properties of model membranes change as a valuable indicator has been provided. The nanomechanics (elasticity) and surface topography (roughness) of model lipid membranes that result from oxidative damage have not yet been quantified at the nanoscale.

2. Results and Discussion

Peer-reviewed version available at Int. J. Mol. Sci. 2019, 20, 2709; doi:10.3390/ijms20112709

2.1. Preparation of mesoporous silica-PEG nanoparticles (MSNs)

2.1.1. Stabilization of mesoporous amine-propyl functionalized MSNs by PEG

The scheme of the MSNs synthesis is presented on the Figure 1.

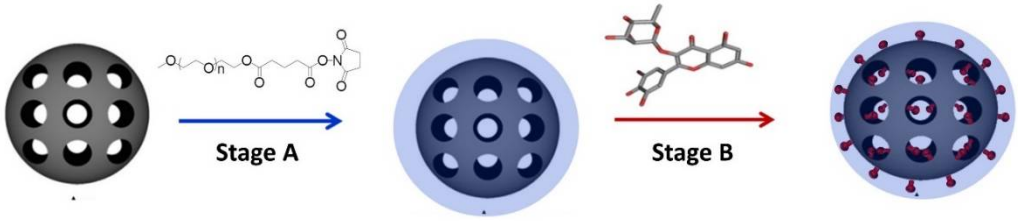

Figure 1. Synthesis of the flavonoid loaded MSNs. Stage A: PEGilation of propylamine MSN; Stage B: loading of flavonoids

Methoxy- poly(ethylene glycol) succinimidyl glutatare (mPEG-SCM) with a molecular weight of 5000 g mol-1 was used in all experiment to PEGylate the pre-coated propyl-amine nanoparticles on the surface. The characterization of propyl-amine nanoparticles used in experiments were characterized by X-ray powder diffraction X-ray diffraction (XRPD), Brunauer-Emmet-Teller (BET) analysis, Atomic force microscopy (AFM), Field emission scanning electron microscope (FE-SEM) and electrophoretic (zeta potential) and dynamic light scattering (DLS) measurements. Data are summarized in Table 1. and Figure 2.

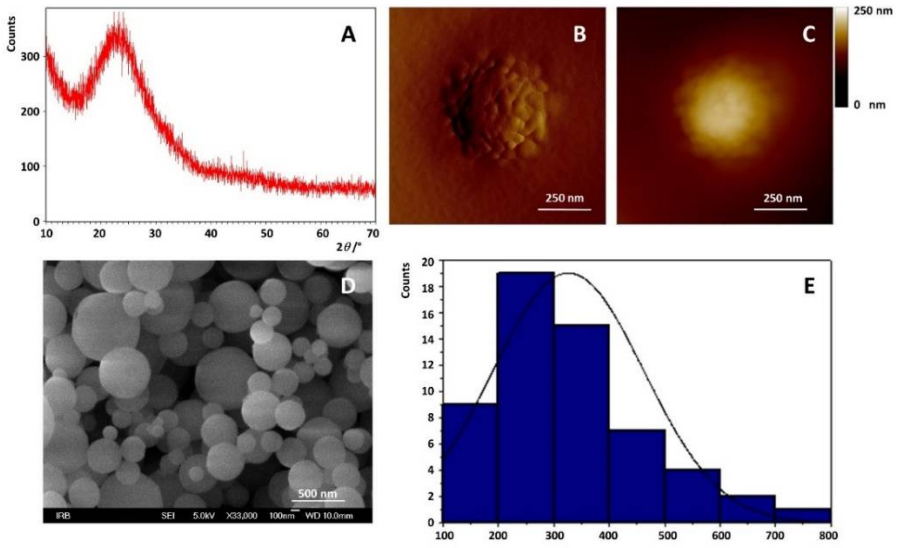

Figure 2. (A) The diffraction pattern of the investigated powdered MSNs, (B) Amplitude and (C) 2D height image of MSNs. (D) FE-SEM micrograph of MSNs as used. (E) The histogram of the size distribution of MSN.

Table 1. The porosity, morphology and stability of MSNs in powder and dispersed in water.

	Specific surface/ m^2 g^{-1}	Specific surface/ m^2 g^{-1}	Pore size/ nm
BET analysis	693.78	0.8368	4.82
Zeta potential / mV		+26±2	
d_H/ nm		913±180	
[1]d/nm		326±137	

[1] FE-SEM (N = 57).

The diffraction pattern of the investigated powdered MSNs is not characterized by sharp diffraction lines but shows a typical halo in the 2 = 20-30° region which proves the amorphicity of the sample i.e. indicates short-range atomic ordering between the Si and O at the prepared MSNs. The distribution of diameters of MSNs obtained on powder sample (Figure 2D) using FE-SEM micrograph amounted (326±137) nm (Figure 2 D, *N*= 57) what is in agreement with the AFM imaging results where the average diameter of observed MSN (Figure 2B and C) has be determined to be around 300 nm, while dispersed MSNs in water tend to aggregate resulting in high increase of the diameter with the hydrodynamic diameter of aggregates obtained by dynamic light scattering (DLS) (dH=913±180) nm. Measured value of the zeta potential (ζ = + 26 ± 2 mV) confirms that the nanoparticles are positively charged and are stable in the aqueous medium. Unmodified MSNs have negative zeta potential, (ζ= - 50 mV) in a wide pH range reflecting the large surface charge due to deprotonated Si-OH groups. Conversely, functionalized MSN with -NH_2, -CH_3, and -OH groups may have a positive, neutral or negative charge, depending on the pH medium [47] . Therefore, in our case, the positive zeta potential comes from the propylamine of MSNs functionality.

We further performed the experiments to stabilize MSNs. PEG is hydrophilic, biocompatible and non-toxic and can therefore delay hydrolysis and enzymolysis [48]. PEG prevents protein adsorption (opsonization) on the surface of NPs and decreases non-specific intake into the reticuloendothelial system [49]. The amount of PEG that can be incorporated into the liposome lipid bilayer decreases with an increase in molecular weight of PEG [50] of 15 mol % in PEG 120 to 5-7 mol % for PEG 2000 and PEG 5000. Above 7.5 mol% for PEG 1900 comes liposome dissolution [51]. The best conditions for avoiding of adsorption of biomolecules to surface MSNs are with long PEG chains and high surface density [52].

Propyl-amine functionalized mesoporous silica nanoparticles 100 mg and 100 mg of methoxy-poly(ethylene glycol) succinimidyl glutarate (m-PEG-SG, MW 5000) are dissolved in 50 mL of ethanol (EtOH). The mixture was stirred for 24 h at 25°C (50 rpm) to induce the formation of covalent bonds between propyl-amine groups on the surface of the mesoporous SiO2 nanoparticles and succinimidyl groups of PEG. After that, the resulting mixture was removed to an ultrasonic bath to keep the mixture homogeneous. The resulting nanoparticles were separated from unreacted mPEG-SCM by five cycles of centrifugation (6000 rpm) and redispersed in ethanol. The dispersion of nanoparticles (MSNs) was left on air overnight to dry.

Part of the samples of PEG-coated MSNs was used for the analysis and the characterization. The results from AFM, FTIR spectroscopy and FF-SEM are depicted on Figure 3.

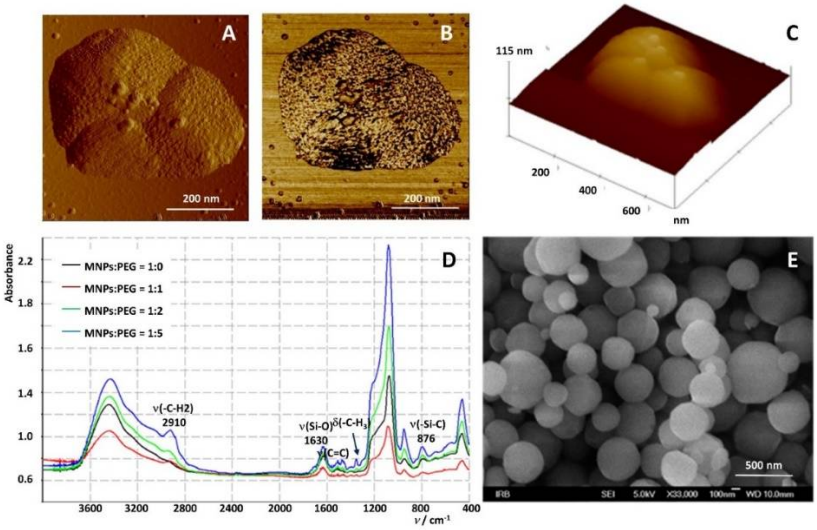

Figure 3. (A) Morphology of MSNs coated with PEG. Top view of the 2D AFM height image, vertical scale 100 nm, (B) phase image indicating PEG coatings on MNS (white color) on the MSNs), (C) 3D height image of aggregate consisting of three MSNs, (D) FTIR spectra of pure MSNs (black); MSNs with PEG coating in weight ratio 1 : 1 (red); 1 : 2 (green); 1 : 5 (blue), (E) FE-SEM micrograph of the PEG coated MSNs.

AFM 2D and 3D height images (Figures 3A and C) and FF-SEM image (Figure 3E) show morphology of mesoporous MSNs coated with PEG (M_w=5000). The PEG coating was confirmed on the phase image (Figure 3C), white color on the surface of the MSN). Fine PEG coating was confirmed by FTIR spectroscopy (Figure 3D) showing MSNs spectra with different mass ratios of PEG. The peak at 2910 cm-1 was assign to methylene stretching (CH_2) in PEG, a ribbon stretching Si-O (1630 cm^{-1}) and Si-C stretching (876 cm^{-1}). Other peaks that do not belong to pure MSN are at 1710, 1507, 1466 and 1352 cm^{-1}. The last two are due to methylene vibrations of angular vibrations. The average hydrodynamic diameter of MSNs dispersed in water was d_H = 932 ± 91 nm (Table 2) indicating MSNs aggregation process within water dispersion of MSNs. Although the results of DLS showed that MSNs were to some extend aggregated, they remained stable for a prolonged time period with a zeta potential of 27 ± 1 mV (Table 2). Applied methods in the characterization of MSNs, namely FF-SEM, AFM, FTIR spectroscopy and dynamic and zeta potential measurements, confirmed the mesoporosity of the prepared nanoparticles, particularly those coated with PEG (Mw 5000) in weight ratio w(MSNs): w(PEG) = 1: 5) as the most stabilized.

Table 2. The zeta potential of MSNs and the average diameter size of aggregates formed by dispersing of MSN in water

	MSN_PEG$_{5000}$
Zeta potential / mV	+27±1
d_H/ nm	932±91

The rest of the MSNs was used further for the loading of flavonoids.

2.1.2. Loading of flavonoids into MSNs

100 mg pegylated MSNs has been added to the 15 mL of saturated solution of quercetin, myricetin and myricitrin and are mixed on a stirrer during 24 h at 40 °C. The optimization of the ratio between weight of added flavonoids and MSNs was performed and the ratio of w(flavonoids) : w(MSNs) = 3:1) has been found as optimal for the best loading efficiency. After completion, the supernatant is removed and the flavonoid loaded MSNs have been washed three times in ethanol (EtOH). Same procedure was repeated (taking 1 mL of DLS suspension, 2 mL of supernatant for DLS, washing with EtOH three times and transferred to a plastic cup to evaporate EtOH overnight). The analyses are performed after EtOH is evaporated and the sample was dried. The characterization of the flavonoid loaded with flavonoids has been performed by AFM, FE-SEM, FTIR spectroscopy and BET analysis.

The experiments were performed to determine the loading efficiency (LE) at one flavonoid MSNs weight ratio, 3:1. The LE for quercetin, myricetin and myricitrin was 27±9 %, 4±2 %, and 8.6±0.6 %, respectively. Figures 4 A, D and G show the morphology of the MSNs loaded with quercetin, myricetin and myricitrin, respectively. They kept the size and the morphology of those before loading. After the loading of MSNs with flavonoids, flavonoid loaded MSNs were washed with EtOH to remove the unadsorbed flavonoids, the part of them stayed adsorbed on the surface of the MSNs and thus induced the aggregation as it is observed on AFM phase images 4 B, E and F. The BET analyses confirmed the loading of flavonoids by decrease in the free specific surface areas, pore volumes and pore sizes (Table 3). Thus the specific surface area decreased from 693.78 m^2 g^{-1} for empty MSNs to 544.58 m^2 g^{-1}, 546.01 m^2 g^{-1} and 562.78 m^2 g^{-1} for MSNs loaded with quercetin, myricetin and myricitrin, respectively. The equal trend was observed for the pore volume and pore

size of MSNs loaded with flavonoids. Aggregates made of a few number of single MSNs (Figure 4) has an active surface that is somewhat smaller than the sum of surfaces of all individual MSNs. The MSNs, if composed of almost rigid spheres, can have only open pores, i.e. anything that enters will eventually find its way out. As determined experimentally the pore sizes were between 4.82 nm and 3.12 nm. Knowing that the characteristic dimensions of a flavonoid molecule are all around 1 nm (its length is slightly below 2 nm, besides the myricitrin molecule as glycone molecule is the largest among them), flavonoid molecules that could be entrapped within the pores thanks to their hydrophobicity and van der Waals forces correspond their sizes. Thus, for the most hydrophilic flavonoids among used, the myricetin shows the highest hydrophobicity, and should have the smallest LE. FTIR spectroscopy measurements (Figure 4 C, F and I) confirmed also successful loading of flavonoids within MSNs. For quercetin loaded MMNPs, band at 1153 cm^{-1} was attributable to the C–O stretching in the aryl ether ring and the C–O stretching in phenol, respectively [53]. Bands at 2930sh, 2857 cm^{-1} were due to CH stretching of PEG. The band at 1379 cm^{-1} belongs to myricetin (Figure 4F), while in spectrum of myricitrin loaded MSNs are present bands 2930, 1507w, 1461w and 1346w cm^{-1}. (Figure 4I). Band at 1346 cm^{-1} belongs present myricitrin.

Table 3. Specific surface area, pore volume, pore size and loading efficiency (LE) for flavonoid loaded MSNs determined by BET analysis and UV/VIS spectroscopy

	Quercetin	**Myricitrin**	**Myricetin**
Specific surface area/m^2 g^{-1}	544.58	546.01	562.71
Pore volume /cm^3 g^{-1}	0.6404	0.6527	0.73
Pore size /nm	4.70	4.78	3.12
LE (%)	27±9 (*N*=6)	8.6±0.6 (*N*=3)	4±2 (*N*=5)

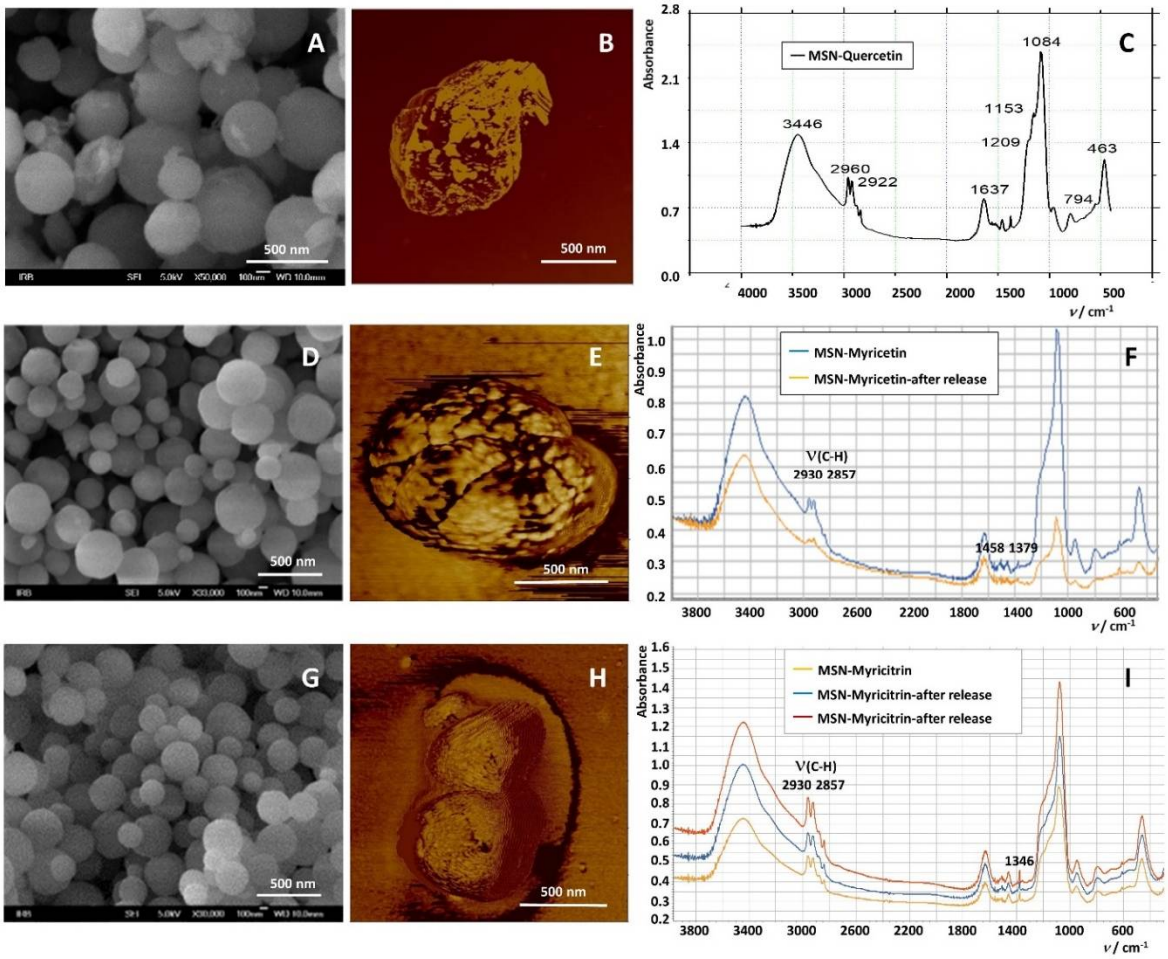

Figure 4. (A, B, C) Characterization of flavonoid loaded MSNs: with quercetin, (D, E, F) myricetin, (G, H I) myricitrin, (A, D, G) FF-SEM of flavonoid loaded MSNs, (B, E, H) AFM phase images, (C, F, I), FTIR spectra of flavonoid loaded MSNs

2.1.3. Release of flavonoids from MSNs

The cumulative release profiles for the selected flavonoids (Figure 5 A and B) are practically unchanged, i.e. essentially not dependent on the flavonoid structure. In early stage of the release, a burst was observed lasting first eight hours. It is thus supposed that around 1.5, 0.4 and 0.5 % of loaded quercetin, myricetin and myricitrin, respectively are situated at the outer surface of MSNs. After 24 hours the release of all three flavonoids changed its character pointing to a different way of the releasing molecules that were adsorbed. Other words, release reached slightly plateau where it is more or less constant. The most flavonoids molecules were thus entrapped into the mesoporous cavities of MSNs. The mechanism of flavonoid release was not specific as already confirmed for the LE meaning that the selected flavonoids were adsorbed to the silica surface via deprotonated catechol groups. Also, after 170 hours only 1.6, 0.45 and 0.55% of quercetin, myricetin and myricitrin, respectively have been released. While within a MSNs flavonoid molecule can last longer, as soon as it is released, its half-life in the medium is only a few days and therefore two competitive processes have to be simultaneously treated during the drug release. The average half-life of quercetin absorbed in a human organism is 3.5 h [54]. The half-life of myricetin at pH 5 PBS buffer is 8 days, while at pH

8 only 0.1 h [55]. The biodegradation half-life of myricitrin is 26 days [56]. The fact that the favonoids loaded into MNSs remained stable during prolonged period of time thus presents a good improvement. Similar improvement in the sense of prolonged release has been found also on quercetin release from poly-lactide NPs showing almost 60% of the released quercetin after 4 days. When quercetin was released from dextran coated NPs the dissolution rate was linear with time with the slope changed after 10 days [18]. The maximum values (70 and 80%, respectively) were achieved after 15 days.

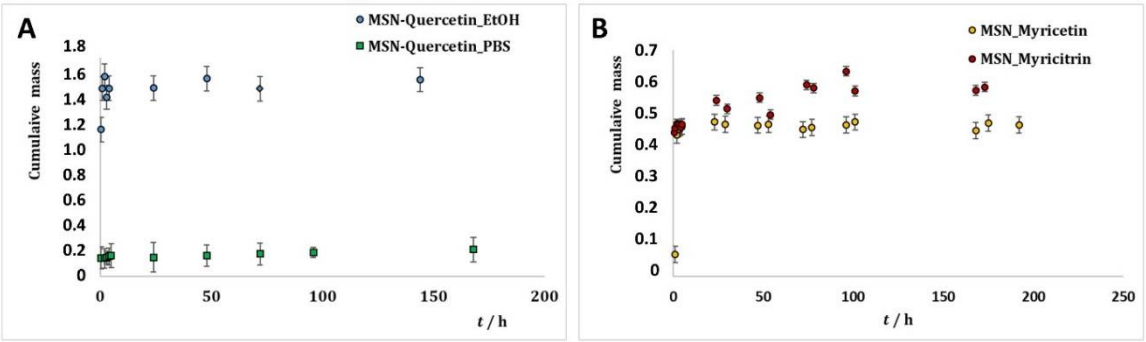

Figure 5. (A) Cumulative release profiles of Quercetin in EtOH/H_2O and PBS, (B), myricetin and myricitrin in EtOH/H_2O

2.2. Interaction of MSNs with model cell membranes

2.2.1. Interaction of flavonoid loaded nanoparticles with model cell membrane

2.2.1.1. Preparation of liposomes

Pure DOPC liposomes were prepared by preparation of stock solutions of dissolved DOPC in chloroform in order to get the mixed solutions with adjusted molar ratio of flavonoid in respect to lipids. After rotary evaporation of the solvents, the remaining lipid films (pure or mixture of flavonoid and lipid in adjusted ratio) were dried in vacuum for an hour and then dispersed by gentle manual shaking at 40 °C in 1 mL of phosphate buffer saline (PBS, pH 7.4, I = 150 mM, containing 137 mM NaCl, 2.7 mM KCl, 1.5 mM KH_2PO_4, 6.5 mM Na_2HPO_4). During rehydration, the lipid film was gradually scraped off the wall of the glass bottle layer by layer and formed cloud-like floaters in the solution. The liposome suspension was left to swell and stabilize overnight at temperature far away from melting point. The final concentration of DMPC in all suspension samples was adjusted to 0.5 mg mL^{-1}. For AFM measurements all supported lipid bilayer (SLB) samples were prepared under the same experimental conditions by the drop deposition method on freshly cleaved mica attached to a metal disc. A volume of 100 µL MLV suspension were pipetted directly onto mica substrate, incubated for 10 min and flushed with filtered (0.22 µm Whatman) PBS solution.

2.2.1.2. Characterization Techniques

In this work, the zeta potential measurements as well as the AFM and force spectroscopy studies were performed to consider the flavonoid effects on the nanomechanical properties of the model membrane as well as to reveal their protective role in induced lipid peroxidation process.

2.2.1.3.The protective role of released flavonoids into model membranes their protective role during H_2O2 induced lipid peroxidation

In order to clarify the effect of the insertion of two distinct flavonoids, myricetin and myricitrin, released from MSNs on the topography, organization and nanomechanical properties of DOPC SLB, using the protocol described in experimental section, we prepared 25 mL DOPC MLV liposome suspension (0.5 mg mL^{-1}) in PBS buffer solution (I = 150 mM, pH = 7.4), in which the membrane bag with empty or flavonoid loaded MSNs (30 mg) has been immersed. During incubation of MSNs within liposome suspension, the system has been mixed every 4 hours to ensure homogenization. After 48 h, the membrane bag was removed from liposome suspension. The loss of lipids and subsequent concentration reduction of lipids and flavonoids during process of extrusion have been avoided by using prepared MLV dispersions without the process of extrusion. The insertion of the flavonoid (quercetin, myricetin and myricitrin) has been checked by AFM measuring of the SLBs. To prepare SLB for AFM imaging and force spectroscopy measurements, the drop of MLV liposome suspension was added to fluid cell with mica plate and kept at 25°C. After liposome adsorption, the remaining liposomes were removed by washing the surface with PBS, and allowed to thermostated at 25°C. The liposome adsorption during sample deposition and liposome spreading over the mica surface during AFM imaging resulted in the formation of continuous uniform SLB as consequence of the sum of the contributions of electrostatic interactions between liposomes and support, the liposome alone as well as the surrounding aqueous medium [34]. The lipid peroxidation process has been induced by the addition of 5 µL H_2O_2 (10^{-5} M and 5 µL 10^{-5} $CuCl_2$) to liposome dispersion 1 h before the formation of the SLB from treated liposomes suspension.

Therefore, our first issue was to answer to the question whether the flavonoids in respect to their difference in hydrophobicity, or structure, and molar ratio towards lipids are able to insert lateral homogeneously in the bilayer. and whether the inserted flavonoids protect the model lipid membrane towards lipid peroxidation process. To get answer to this question, we performed zeta (ELS), AFM and force spectroscopy measurements.

The insertion of the flavonoid (quercetin, myricetin and myricitrin) has been checked by zeta potential measuring of the prepared DOPC liposomes, without and with inserted flavonoids. The obtained results are presented in Table 4. as average value ± standard deviation of five independent measurements for each sample. Recalling the zeta potential of the pure DOPC liposomes (ζ = -4.2 mV) [57] and comparing it with zeta potentials of DOPC liposomes with flavonoid loaded MSNs, we concluded that in all cases, flavonoids released from MSNs during incubation with DOPC liposome at 25 °C, were inserted into the DOPC bilayer as denoted by the shift of the zeta potential to negative values (from −6.1 ± 1.1 mV for pure DOPC to -14.4±4.7 mV, -6.7±1.3 mV and -11.8±3.2 mV for quercetin, myricetin and myricitrin, respectively. The similar behaviour has been observed in the study of interaction of glucone hysperidin and aglicone hesperitin with DMPC bilayer [38], in that has been established that insertion of flavonoids followed by changes in zeta potential values, that turns down near saturation of bilayer with flavonoids. However, the valuable information could be throw up from the results shown above and sufficient for following conclusion. First, as shown in this study for DOPC in PBS buffer solution, the electrophoretic mobility of DMPC liposomes are low, but not negligible. Our result obtained in flavonoid/DOPC study (ζ =-6.21±1.1 mV at 25 °C for fluid phase) is in agreement with already reported (ζ =-4.2 mV) [57] confirming the proper sample

preparation and the reproducibility of the results. The net negative zeta potential value in PBS buffer solution confirmed the binding of the ions present in the buffer solution at I = 0.15 M. Second, recalling of the pK_a = 5.87 and 8.48 [58], pK_a = 6.33 [59] and pK_a = 5.23 [60] for quercetin, myricetin and myricitrin, respectively, the anion species of quercetin, myricetin and myricitrin (deprotonated species) are predominant at pH 7.4. The shift in zeta potential towards negative values might be ascribed only to the addition of flavonoids. This is taken as a strong indication that the increase in the surface negative charge is due to flavonoid insertion into the DOPC liposomes. After addition of H_2O_2, zeta potential shifts towards positive values have been observed from –14.4±4.7 mV to -8.1± 1.4 mV and from -11.8±3.2 mV to -6.2±2 mV for quercetin and myricitrin, respectively. In contrast, the shifts towards more negative zeta potential have been observed from -6.1±1.1 mV to -17.8±6 mV and from -6.7±1.3 mV to -10.4±2.2 mV for pure DOPC and myricetin, respectively. That could indicate that the mechanism of membrane protection occurred different for structurally different flavonoids in respect to their location within the membrane. It is important to highlight that the shift in zeta potential values were suppressed in the presence of the flavonoids ($\Delta\zeta$ = +6.3±6.1 mV, $\Delta\zeta$ = -3.7±3.5 mV and $\Delta\zeta$ = +5.5±5.2 mV) for quercetin, myricetin and myricitrin, respectively, in comparison to pure DOPC liposomes ($\Delta\zeta$ = -11.7±7.6 mV). These measurements in some extend the protective role of used flavonoids under induced oxidative stress.

Table 4. Zeta potential values of DOPC liposomes (γ= 0.5 mg mL^{-1}) with and without inserted flavonoids at 25 °C before and after induced lipid peroxidation process by addition of H_2O_2

Sample	DOPC	DOPC/Quercetin loaded MSNs	DOPC/Myricetin loded MSNs	DOPC/Myricitrin loaded MSNs
$^1\zeta$/mV	−6.1 ± 1.1	-14.4±4.7	-6.7±1.3	-11.8±3.2
$^2\zeta$/mV	−17.8 ± 6	-8.1±1.4	-10.4±2.2	-6.3±2

[1] before addition of H_2O_2, [2] after addition of H_2O_2.

Therefore, our next issue was to answer to the question whether the flavonoids in respect to their difference in hydrophobicity and structure towards lipids are able to insert lateral homogeneously in the bilayer. To get answer to this question, we performed AFM measurements. The topography of SLB with inserted flavonoid before and after addition of H_2O_2 and Cu^{2+} ions in PBS obtained for different samples at 25°C is presented in Figure 6. By adjusting the pH = 7.4, the time and conditions of imaging, the formation of SLB was optimized and therefore the changes in topography of the SLB correspond only to the differences between the samples. The cross sections profiles show the profiles correspond to the single supported bilayer covering the mica support (Figure S1).

Peer-reviewed version available at Int. J. Mol. Sci. 2019, 20, 2709; doi:10.3390/ijms20112709

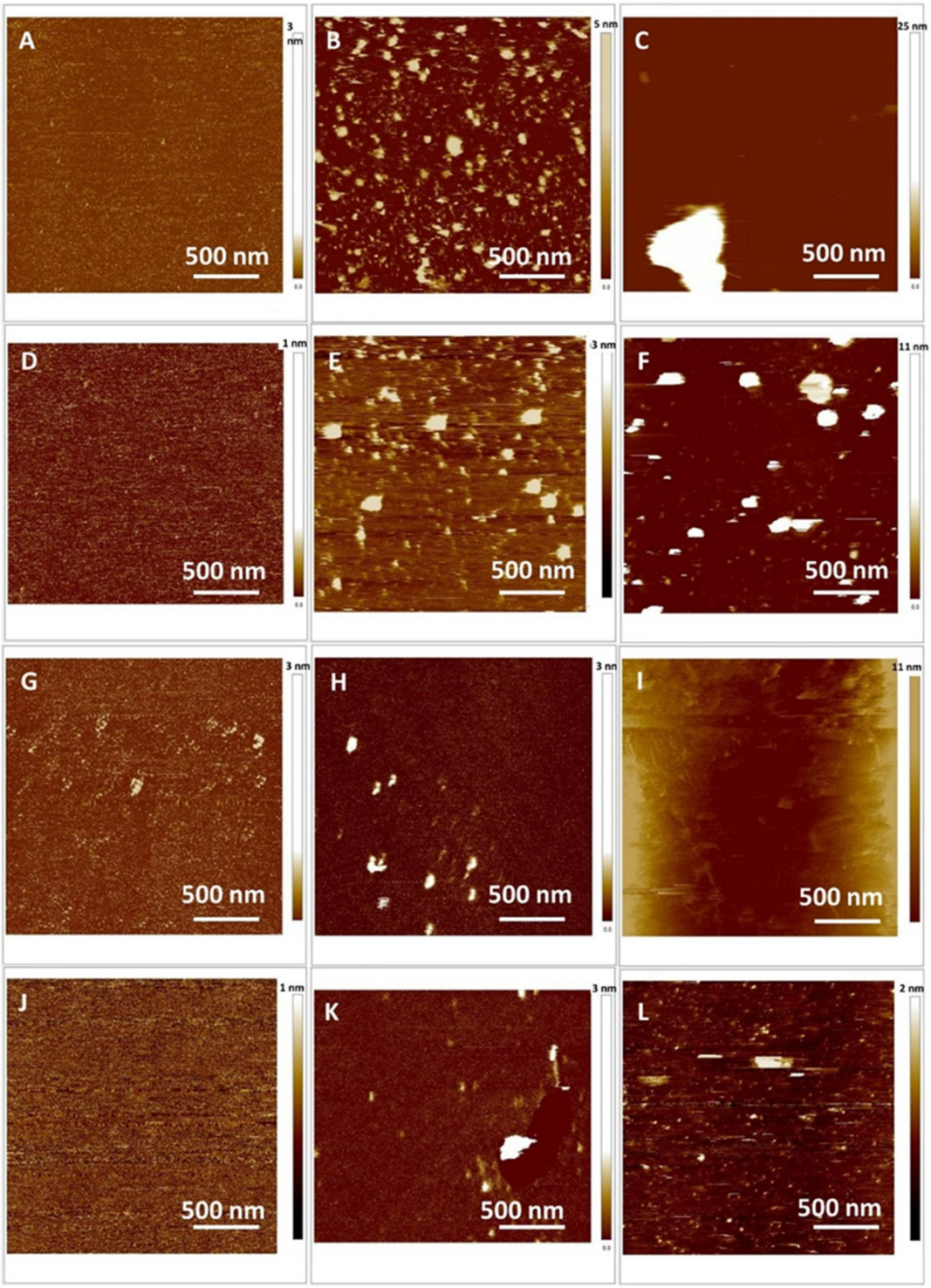

Figure 6. Top view of 2D height AFM images on the model (DOPC) SLB: (A, B, C) control, (D, E, F) quercetin loaded DOPC; (G, H, I) myricetin loaded DOPC, (J, K, L) myricitrin loaded DOPC. The lipid peroxidation induced by (B, E, H, K) H_2O_2, (C, F, I L) H_2O_2 and Cu^{2+}.

The homogeneous scabrous SLBs without ruptures are clearly seen irrespective of inserted flavonoids. The roughness of the SLB for all examined protrusions from the unperturbed SLB surface are corrected for the convolution effect of the tip [61] and presented in Table 5. The roughness of the

Peer-reviewed version available at Int. J. Mol. Sci. 2019, 20, 2709; doi:10.3390/ijms20112709

different domains of the SLBs has been calculated by four random average root mean square (R_a) values on area 2×2 μm^2.

The average roughness of control DOPC SLB amounts Ra = 0.08±0.01 nm indicating very smooth SLB, while the moderately rougher surface of SLBs exposed MSNs containing quercetin, myricetin, and myricitin showed roughness R_a = 0.11±0.05 nm, 0.12±0.06 nm and 0.19±0.09 nm, respectively. This difference in the roughness in comparison to the control DOPC SLB (ΔR_a = 0.03, 0.04 and 0.14 nm for quercetin, myricetin and myricitrin, respectively) could be explained only by increased surface density of the observed protrusions on the investigated area (25 μm^2 caused only by insertion of flavonoids. Recalling the hydrophobicity/hydrofilicity i.e. partition coefficients of examined flavonoids (log P = 1.86, 1.75 and for quercetin, myricetin and myricitrin, respectively) [62], the significant higher roughness has been observed for more hydrophilic flavonoid glucone myricitrin in comparison to other. Since the all SLB were performed under the same experimental conditions, the observed difference in roughness value seems to be good indicator for the incorporation of the released flavonoids from the MSNs into the DOPS liposomes during 48 hours of exposure.

Now we turn back to the question of the effects of the flavonoid on the nanomechanical properties of DOPC SLB. The effect of flavonoids on the nanomechanics was further investigated in detail by force spectroscopy. The elasticity maps (Figure 7) showed a values of the elasticity that can be attributed to the fluid phase of DOPC. A distinct decrease of the Young modulus was observed from E =63.7±5.2 MPa (for control DOPC SLB) to E = 40.6±2.7 MPa, 31.4±2.9 MPa and 37.6±4.8 MPa (for quercetin, myricetin and myricitrin, respectively exposed pure DOPC). The observed decrease in Young moduli of SLB indicated insertion of exposed flavonoids hosted in MSNs that have been released during incubation time. However, the insertion of the flavonoids occurred without any impact on SLB morphology and homogeneity, i.e. reduced membrane stiffness (or absence of elasticity) has not been enough to disorganize or destabilize the whole SLB structure by pore formation. These behaviours could be attributed to the decreased lipid lateral interactions in PBS provoked by the insertion of the flavonoids. The observable increased fluidities of the DOPC SLB with inserted flavonoids with respect to the pure DOPC SLB amounted ΔE = -23.1 ±7.9 MPa, 32.3±8.1 MPa and 26.1±10.0 MPa for quercetin, myricetin and myricitrin, respectively. Without taken in consideration the concentration of released flavonoids during 48 h, at the same experimental conditions, the highest effect on the elasticity of DOPC SLB showed hydrophobic aglycone myricetin indicating that the affinity or activity of myricetin to DOPC SLB appeared higher than other two flavonoids. By analogy recent reported studies on SLBs with aglycone hesperetin and glycone hesperidin [38, 63], the permeation is not expected to be equal for the glycone myricitrin and aglycone myricitrin. This indicates that bilayer disordering was caused by the flavonoid presence as well as the insertion of the flavonoids is in agreement with corresponding partition coefficients. The presence of flavonoids, particularly hydrophilic myricitrin near the lipid phosphate groups modified the orientation of the bilayer dipoles and consequently the mutual interaction between the phospholipids. On the other side, the inclusion of flavonoids, at low concentrations conditions showed moderate effect on lipid rearrangement, causing the expansion of the nonpolar domains within the bilayer and thus the increase in the membrane elasticity.

Peer-reviewed version available at Int. J. Mol. Sci. 2019, 20, 2709; doi:10.3390/ijms20112709

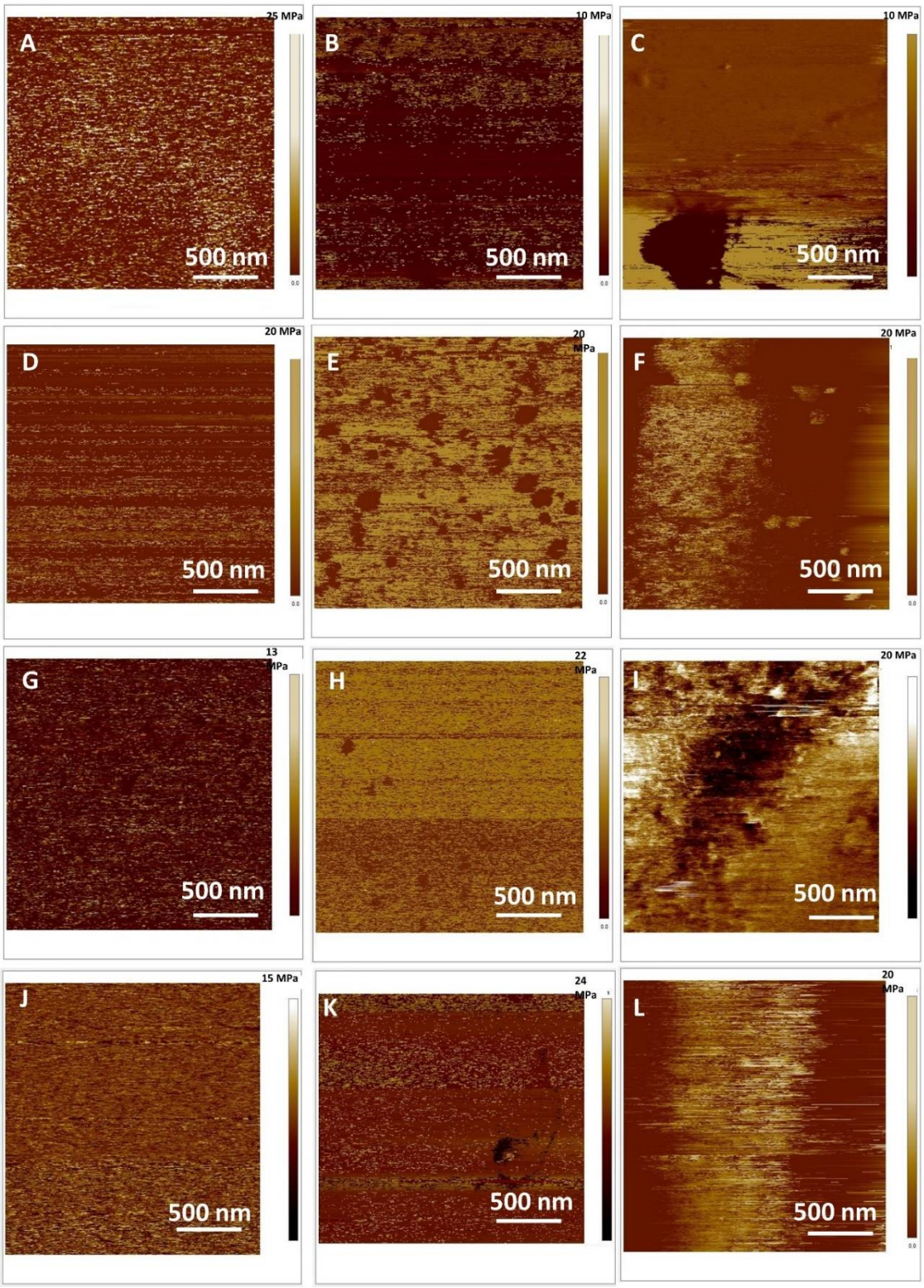

Figure 7. Young modulus maps of the model lipid (DOPC) SLB: (A, B, C) control; (D, E, F) quercetin loaded DOPC, (G, H, I) myricetin loaded DOPC, (J, K, L) myricitrin loaded DOPC. The lipid peroxidation induced by (B, E, H, K) H_2O_2, (C, F, I L) H_2O_2 and Cu^{2+}.

Our next issue was to answer to the question whether the inserted flavonoids protect the model lipid membrane towards induced lipid peroxidation process by addition of H_2O_2 and Cu^{2+} ions. To get answer to this question, we performed further AFM and force spectroscopy measurements and analysis.

The topography of SLB with inserted flavonoid after addition of H_2O_2 and Cu^{2+} ions in PBS obtained for different samples at 25°C is presented in Figures 6. (E, H K) and Figures 6. (C, F, I, L), while the cross sections profiles show the profiles correspond to the single supported bilayer covering the mica support (Figure S1.). Opposite to pure DOPC SLB, the inhomogeneous scabrous SLBs with protrusions are clearly seen irrespective of inserted flavonoids. The average roughness of pure DOPC SLB exposed to H_2O_2 and H_2O_2 and Cu^{2+} ions showing the quite rough surfaces increased from R_a = 0.08±0.01 nm to R_a = 0.33±0.05 nm and R_a = 0.84±0.02 nm, respectively, indicating significantly disrupted surface during lipid peroxidation process. The increases of the roughness have been shown to be ΔR_a = +0.25±0.06 nm and ΔR_a = 0.76±0.01 nm, for addition of H_2O_2 and H_2O_2 and Cu^{2+} ions, respectively. The same, but reduced effect of the induced lipid peroxidation process was observed in all SLBs with inserted flavonoids, indicating the protective role of flavonoids towards lipid peroxidation. The damage of the SLB induced by the H_2O_2 addition was reduced from ΔR_a =+0.25±0.06 nm to ΔR_a =0.07±0.11 nm, 0.10±0.08 nm and 0.11±0.13 nm for treated SLBs by quercetin, myricetin and myricitrin, respectively. The protective role of the present flavonoids is also observable in the treatment of SLBs with H_2O_2+Cu^{2+}, but the protection is much more suppressed indicating a different mechanism of the process of lipid peroxidation (Table 5).

Table 5. The effect of induced lipid peroxidation on the roughness (Ra) and the Young Modulus (E) of the model DOPC SLB (N=6)

Sample	R_a / nm	Δ R_a /nm	E / MPa	Δ E / MPa
Control DOPC	0.08±0.01		63.7±5.2	
Control DOPC /H_2O_2	0.33±0.05	+0.25±0.06	41.5±3.9	-22.2±9.1
Control DOPC / H_2O_2+ Cu^{2+}	0.84±0.02	+0.76±0.01	38.2±4.1	-25.5±9.3
DOPC/Quercetin	0.11±0.05		40.6±2.7	
DOPC/Quercetin / H_2O_2	0.18±0.06	+0.07±0.11	35.5±1.6	-5.1±4.3
DOPC/Quercetin / H_2O_2+ Cu^{2+}	0.81±0.17	+0.70±0.22	16.6±7.4	-9.2±9.0
DOPC/Myricetin	0.12±0.06		31.4±2.9	
DOPC/Myricetin/ H_2O_2	0.22±0.02	+0.10±0.08	25.3±2.8	-6.1±.5.7
DOPC/Myricetin/H_2O_2+ Cu^{2+}	1.02±0.05	+0.80±0.07	17.6±2.1	-13.8±5.0
DOPC/Myricitrin	0.19±0.09		37.6±4.8	
DOPC/Myricitrin/ H_2O_2	0.30±0.04	+0.11±0.13	18.8±4.3	-18.8±.9.1
DOPC/Myricitrin/ H_2O_2+ Cu^{2+}	0.81±0.04	+0.62±0.13	14.7±3.4	-22.9±8.2

Mutually comparing the protection of SLBs by insertion of different flavonoids, it could be concluded, that the quercetin had the highest protective activity measured by the roughness parameter. The structural reorganization of the lipid molecules and the SLB damage during and after lipid peroxidation are reflected in the Young moduli values obtained during force spectroscopy measurements. The values are presented in Table 5. The elasticity maps shown on Figures 7 B, E, H,

K present fluid DOPC SLBs after addition of H_2O_2, while Figures 7 C, F, I and L show elasticity maps of fluid DOPC SLBs after addition of H_2O_2 and Cu^{2+} ions. After addition of H_2O_2, distinct decreases of the Young modulus were observed from 63.7±5.2 MPa to 41.5±3.9 MPa for control DOPC SLB (ΔE = -22.2±9.1 MPa). The similar, but increased change (ΔE= -25.5±9.3 MPa) was observed also after addition H_2O_2 + Cu^{2+} ions. The shifts in elasticity at the presence of flavonoids after addition of H_2O_2 were significantly supressed (ΔE= -5.1±4.3 MPa, ΔE= -6.1±5.7 MPa and (ΔE =-18.8±9.1 MPa for quercetin, myricetin and myricitrin, respectively. The observed decrease in Young moduli of SLB confirmed the insertion of exposed flavonoids hosted in MSNs that have been released during incubation time and their protective role during lipid peroxidation. Other words, the softening of the SLBs during lipid peroxidation was significantly reduced. The protective ability of the quercetin seems to be the highest among used flavonoids. The same, but somewhat decreased effect was observed also after addition of H_2O_2 and Cu^{2+} ions.

In conclusions, the present study shows a differential alternating effect of used flavonoids, namely, quercetin, myricetin and myricitrin on behaviour of DOPC model membranes before and after lipid peroxidation process. Without taken in consideration flavonoid location in respect to their structure and hydrophobicity, they possess distinct anti-oxidative capacity in protection of model membrane towards damage and disordering of the lipid molecules within the membrane maintaining its elasticity and functionality as best as possible. This results should be taken into consideration in order to understand lipid- flavonoid interaction, ROS-flavonoid- lipid mutual interactions, however further works are necessary in order to understand the anti-oxidative mechanism on the higher organisation level as the cells present.

3. Materials and Methods

3.1. Materials

Propylamine functionalized silica mesoporous nanoparticles, 200 nm particle size, pore size 4 nm, methoxy poly(ethylene glycol) succinimidyl glutarate (average molecular weight 5000 g/mol, were purched from Sigma-Aldrich and used as received, 1,2-dioleoyl-sn-glycero-3-phosphocholine (DOPC (18:1), Avanti Polar Lipids Inc., USA, >99% purity) was used as received for liposome preparation for AFM and zeta potential measurements. All chemicals were of the highest purity commercially available. Kvercetin (Mr= 302.24 g mol-1, Sigma Aldrich), Myricetin (Mr = 318.23 g mol-1, Sigma–Aldrich), Myricitrin (Mr = 464.38 g mol-1, Sigma–Aldrich), Chloroform ($CHCl_3$, Lach-ner, Czech Republik, >99.5% purity), ethanol (Sigma Aldrich, >99% purity), methanol (MeOH, Lach-ner, Czech Republik, >99.5%) and phosphate buffer saline tablets (PBS, pH 7.4, I = 150 mM, containing 137 mM NaCl, 2.7 mM KCl, 1.5 mM KH_2PO_4, 6.5 mM Na_2HPO_4, Sigma-Aldrich) , H_2O_2 (Kemika, Zagreb) and $FeCl_2$ (Sigma Aldrich) were used as received for nanoparticles, film and dispersion preparation for AFM and IR spectroscopy measurements.

3.2. Methods

3.2.1. Characterization of MSNs

3.2.1.1. Field emission scanning electron microscope (FE-SEM)

Field emission scanning electron microscope (FE-SEM) JSM-7000F (JEOL) was used for the observation of particle morphology. The FE-SEM was connected to the Oxford Instruments EDS/INCA 350 energy dispersive X-ray analyzer for elemental analysis. Samples dispersed at an appropriate concentration were cast onto a glass sheet at room temperature and imaged.

3.2.1.2. The MSNs size distribution

The size distribution was determined using Image-J (Media Cybernetics, USA) by measuring diameters of at least 500 MSNs based on FE-SEM images and presented as a histogram of the nanoparticle diameters.

3.2.1.3. X-ray powder diffraction X-ray diffraction (XRPD)

Here, X-ray diffraction in polycrystalline is used to determine crystalline size, crystal and amorphous material differentiation and to solve and crystallize the crystalline structure. In diffraction structural analysis, monochromatic x-ray radiation with small wavelengths is used in the range from = 0.05 to 0.25 nm. Since the λ of X-rays approximates the size of the atoms, this radiation is suitable for determining the structural arrangement of the atoms and molecules of different materials. The position of the diffraction maximum is determined by the crystal grating, the size and form of the unit grid, and the intensity of the diffraction peak atoms of the atom and their spatial deployment in the unit cell according to the requirements of the symmetry, i.e. the crystal structure. In addition to determining the position of the diffraction lines that are directly related to the size and shape of the unit grid, a lot of additional information is obtained from the data which affects all the intensity of the individual maximum lines. The structural features of the prepared sample were studied and characterized by powdered X-ray diffraction at room temperature using a Philips MPD 1880 diffractometer with monochromatic CuK a radiation (λ = 0.1541 nm). All samples were recorded at angle 2-15 in the range of 10-70° with a 0.02° step with a fixed time of 10 s per step.

3.2.1.4. Fourier-transform infrared spectroscopy (FTIR spectroscopy)

FTIR spectroscopy is a technique used to obtain an infrared spectrum of a solid, liquid or gas. An FTIR spectrometer simultaneously collects high-spectral-resolution data over a wide spectral range. This confers a significant advantage over a dispersive spectrometer, which measures intensity over a narrow range of wavelengths. The term Fourier-transform infrared spectroscopy originates from the fact that a Fourier transform (a mathematical process) is required to convert the raw data into the actual spectrum. FTIR spectra were measured on an ABB Bomem MB102 spectrometer, equipped with CsI optics and a DTGS detector. All spectra were collected with a nominal resolution of 4 cm^{-1} and 32 scans at 25 °C. The samples were dried and mixed with KBr to be compressed to a plate for measurement.

565 *3.2.1.5. Atomic Force microscopy*

566

567 The MSNs topography and morphology was determined using theMultiMode Scanning Probe
568 Microscope with Nanoscope IIIa controller (Bruker, Billerica, USA) with SJV-JV-130V ("J" scanner
569 with vertical engagement); Vertical engagement (JV) 125 μm scanner (Bruker Instruments, Inc). 4 μL
570 of the MSNs dispersion (20 mg/mL) was deposited directly onto the freshly cleaved mica (Mica Grade
571 V-4, 9.9 mm disc) mounted on SPM Sample Mounting Disc. After 60 s mica surface has been washed
572 out with 100 μL Milli-Q water in order to remove unadsorbed MSNs. The washing procedure has
573 been repeated two times. The mica surface was dried in air 3 hours. The AFM imaging was performed
574 in Tapping Mode under ambient conditions in air using R-TESPA probe Bruker, Billerica, USA,
575 Nom. Freq. 300 kHz, Nom. spring constant of 40 N/m. The tapping force, calculated as the ratio of
576 engaged to free amplitude cantilever oscillations (A/A_0) has been maintained at low force (0.8-0.9)
577 which is appropriate for the study of soft and deformable samples. The linear scanning rate was
578 optimized between 1.0 and 1.48 Hz at the scan angle 90°. Imaging and collecting the data have been
579 performed with maximal pixel number (512×512). The analysis of images has been performed using
580 the offline AFM NanoScopeTM software (Digital Instruments, Santa Barbara, CA, Version V614r1
581 and V531r1). All images are presented as raw data except for the first-order two-dimensional
582 flattening.

583

584 *3.2.2. Loading of flavonoids into MSNs*

585

586 The significant surface area, high pore volume and pore size of the synthesized MSPs ensure to
587 access their potential to be promising drug delivery vehicles for flavonoids. Loading of flavonoids
588 was performed in pure ethanol. 30 mg MSNs was added to 30 mL flavonoid saturated solution. The
589 suspension of MSNs is stirred for 24 h to allow for diffusion into the pores. Flavonoid loaded MSNs
590 were separated by applying centrifuge and dried in desiccator overnight. Successful loading of
591 flavonoids was confirmed by UV/VIS spectroscopy, zeta potential measurements, Brunauer-Emmet-
592 Teller (BET) analysis and Fourier transform infrared (FTIR) spectroscopy.

593

594 *3.2.2.1. UV/VIS spectroscopy*

595

596 The Beer-Lambert law (or Beer's law) is applied to determine the amount of flavonoids loaded
597 into MSNs, UV/VIS spectroscopy was employed to directly measure the flavonoid concentration loss
598 in pure EtOH supernatant above synthesized MSNs measuring the absorbance at wavelength λ= 375
599 nm). Compared with flavonoid concentration supernatant before adding the synthesized MSNs, the
600 concentration loss was determined using calibration curve in pure EtOH (Figures S3.). All
601 measurements for quercetin, myricetin and myricitrin were performed at temperature 25 °C and λ =
602 380 nm, λ = 375 and λ = 380 nm, respectively. The loading efficiency (LE), the ability of the material
603 to entrap a certain active substance is defined as the ration between weight of the losded flsvonoid
604 into MSNs and the weight of the MSNs.

605

606

607 *3.2.2.2. Zeta potential measurements*

608

609 The zeta (ξ) potential of MSNs was measured using a Zetasizer Nano ZS (Malvern, UK)
610 equipped with a green laser (532 nm) using the M3-PALS technique. All measurements were
611 conducted at 25 °C. Data processing was done by the Zetasizer software 6.32 (Malvern instruments).
612 Results are reported as an average value of 3 independent measurements.

613

614 *3.2.2.3. Brunauer-Emmet-Teller (BET) analysis for MSNs porosity determination*

615

616 Nitrogen adsorption-desorption measurements were performed on an ASAP2020
617 (Micromeritics, USA) accelerated surface area analyzer at 77 K. Before measuring, the samples were
618 degassed in a vacuum at 120 °C for at least 6 h.

619

620 *3.2.2.4. Fourier-transform infrared spectroscopy (FTIR spectroscopy)*

621

622 FTIR spectroscopy is a technique used to obtain an infrared spectrum of a solid, liquid or gas.
623 An FTIR spectrometer simultaneously collects high-spectral-resolution data over a wide spectral
624 range. This confers a significant advantage over a dispersive spectrometer, which measures intensity
625 over a narrow range of wavelengths. The term Fourier-transform infrared spectroscopy originates
626 from the fact that a Fourier transform (a mathematical process) is required to convert the raw data
627 into the actual spectrum. FTIR spectra were measured on an ABB Bomem MB102 spectrometer,
628 equipped with CsI optics and a DTGS detector. All spectra were collected with a nominal resolution
629 of 4 cm^{-1} and 32 scans at 25 °C. The samples were dried and mixed with KBr to be compressed to a
630 plate for measurement.

631

632 *3.2.3. Release kinetics of flavonoids from MSNs*

633

634 *3.2.3.1. UV/VIS spectroscopy*

635

636 The release kinetics of flavonoids from the MSNs (60 mg) in 30 mL PBS or EtOH/PBS (vol. 50/50) was
637 quantified by UV/VIS absorption measurements (Varian Cary 100 Bio spectrophotometer, 10 mm
638 quartz cuvettes) of the supernatant solution (1.5 mL) during 160 h, 80 h and 175 h for quercetin,
639 myricetin and myricitrin, respectively. Each aliquot of measured supernatant was replaced with same
640 aliquot (1.5 mL) of fresh PBS or mixture EtOH/PBS (vol. 50/50) for maintaining the volume of the
641 supernatant constant. Temperature in the measuring compartment was controlled and maintained at
642 25 °C. The calibration curve was drawn by dissolving different amounts of flavonoids in PBS or
643 mixture EtOH/PBS (vol. 50/50) and after filtration of supernatant through filter (F2613-3, PTFE 0.45
644 μm) measuring the peak maximum in the UV absorption spectra (λ_{max}= 375 nm). The linearity of
645 calibration was found to be valid from 1×10^{-6} mol dm^{-3} to 1×10^{-4} mol dm^{-3} with correlation coefficients
646 for quercetin all approaching to 1.00.

647

648

Peer-reviewed version available at Int. J. Mol. Sci. 2019, 20, 2709; doi:10.3390/ijms20112709

649 3.2.3.2. *Zeta potential measurements*
650
651 The change in the zeta potential of MSNs before and after their exposure to feeding solution
652 indicated successful flavonoid loading. The zeta ( ) potential of MSNs was measured using a
653 Zetasizer Nano ZS (Malvern, UK) equipped with a green laser (532 nm) using the M3-PALS
654 technique. All measurements were conducted at 25 °C. Data processing was done by the Zetasizer
655 software 6.32 (Malvern instruments). Results are reported as an average value of 3 independent
656 measurements.
657
658 *3.2.4. Protective role of flavonoids during lipid peroxidation induced by addition of H_2O_2*
659
660 *3.2.4.1. Incorporation of flavonoids into the liposomes and their protective role during lipid peroxidation*
661
662 Pure DOPC liposomes were prepared by dissolution DOPC in chloroform. After rotary
663 evaporation of the solvents, the remaining lipid films were dried in vacuum for an hour and then
664 dispersed by gentle manual shaking at 40 °C in 1 mL of phosphate buffer saline (PBS, pH 7.4, I = 150
665 mM, containing 137 mM NaCl, 2.7 mM KCl, 1.5 mM KH_2PO_4, 6.5 mM Na_2HPO_4). During rehydration,
666 the lipid film was gradually scraped off the wall of the glass bottle layer by layer and formed cloud-
667 like floaters in the solution. The liposome dispersion was left to swell and stabilize overnight at
668 temperature far away from melting point. The final concentration of DOPC in all dispersion samples
669 was adjusted to 0.5 mg mL^{-1}. For AFM measurements all supported lipid bilayer (SLB) samples were
670 prepared under the same experimental conditions by the drop deposition method on freshly cleaved
671 mica attached to a metal disc. A volume of 100 mL MLV dispersions were pipetted directly onto
672 substrate, incubated for 10 min and flushed with filtered (0.22 μm Whatman) PBS solution.
673 The incorporation of flavonoids into the liposomes was performed by immersion of flavonoid
674 loaded MSNs (60 mg) placed within Standard RC Membrane into 30 mL DOPC liposome dispersion
675 during 24 h. The release of flavonoids from MSNs and their incorporation into the DOPC liposomes
676 before and after addition of H_2O_2 and Cu^{2+} ions was quantified by AFM and force spectroscopy
677 measurement.

678 *3.2.4.2. Atomic force microscopy imaging in fluid and force spectroscopy before and after induced oxidative*
679 *stress*

680 AFM images were obtained by scanning the supported lipid bilayers on mica surface in fluid
681 using AFM FastScan Dimension (Bruker Billerica, USA) operated using the new PeakForce QNM
682 mode. Imaging was performed under 25.0 °C for the supported lipid bilayers. The temperature that
683 sensor displays, and the real temperature of the sample were adjusted so there was not the
684 temperature gradient between the displayed and the real temperature. Therefore, the calibration of
685 the temperature individual sample holders was unnecessarily. In our AFM experiment in a liquid
686 environment, the mica sample is glued directly to the metallic holder. The whole sample remains
687 attached to the microscope scanner by a magnet. The AFM was allowed to equilibrate thermally
688 before each sample imaging. The AFM measurements were obtained using Scanfastsyst-Fluid+
689 Bruker probes having the spring constant (Nom. k = 0.7 Nm^{-1}; Nom. resonant freq. ν = 150 kHz). The

Peer-reviewed version available at Int. J. Mol. Sci. 2019, 20, 2709; doi:10.3390/ijms20112709

deflection sensitivity has been calibrated, but not the tip radius (the nominal value has been used; *R* = 2 nm). AFM images were collected at random spot surface sampling (at least four areas per sample) for each analysed sample. The quantitative mechanical data was obtained by measuring DMT modulus/Pa using Bruker software. All images are presented as raw data except for the first-order two-dimensional flattening. Processing and analysis of raw data were carried out using the NanoScope Analysis software (Version 1.90). To obtain the Young's Modulus, the retract curve is fit using the Derjaguin-Muller-Toporov model (DMT Modulus) [Roa, 2011].

3.2.4.3. Zeta potential measurements before and after addition of H_2O_2

The zeta ( ) potential of empty and flavonoid-loaded DOPC liposomes in PBS with the pH adjusted previously (pH = 7.4) were measured using a Zetasizer Nano ZS (Malvern, UK) equipped with a green laser (= 532 nm) using the M3-PALS technique. All measurements were conducted at 25.0±0.1 °C. Data processing was done by the Zetasizer software 6.32 (Malvern instruments). The potential was calculated from the measured electrophoretic mobility by means of Henry's equation using the Smoluchowski approximation (f(Ka) = 1.5). Results are reported as an average value of 4 independent measurements.

4. Conclusions

Obtained results will significantly improve understanding of interactions between model membranes with flavonoids (free or loaded in MSNs) and will provide an insight into the molecular mechanisms of flavonoid protective activity. Mesoporous silica structures could be considered as universal, and promising drug delivery material particularly able to load and release with respectable efficiency flavonols of different physico-chemical and/or structural properties. Upon therapeutic intervention with flavonoid loaded MSNs, significant membrane protection can be achieved. The AFM analysis revealed that flavonoid suppressed H_2O_2-provoked changes in model membrane elasticity and its morphological properties, thus confirming its neuroprotective activity. The obtained results indicate the potential of AFM-measured parameters as a biophysical marker of oxidative stress-induced membrane degeneration. In general, this study suggests that AFM should be used as a highly valuable technique in other biomedical applications aimed at screening and monitoring of drug-induced effects at membrane level that should be extend to cellular level.

.

Supplementary Materials:

Figure S1. 3D height AFM maps of the model lipid (DOPC) SLB: (A, B, C) control; (D, E, F) quercetin loaded DOPC; myricetin loaded DOPC (G, H, I) and myricitrin loaded DOPC (J, K, L). The lipid peroxidation induced by H_2O_2 (B, E, H, K) and H_2O_2 and Cu^{2+}.

Figure S2. Cross-section profiles of the model lipid (DOPC) SLB: (A, B, C) control; (D, E, F) quercetin loaded DOPC; myricetin loaded DOPC (G, H, I) and myricitrin loaded DOPC (J, K, L). The lipid peroxidation induced by H_2O_2 (B, E, H, K) and H_2O_2 and Cu^{2+}.

Figure S3. Calibration curve for the transition with maximum at 380 nm of quercetin (A), myricetin (B) and myricitrin (C) UV-VIS spectra of querctin in EtOH (450-280 nm) for solution 2,3,4 and 5 (used in calibration curve, in supernatant (Q-sn), in saturated solution (6Qsat) concentration (D)

Supplementary materials can be found at www.mdpi.com/xxx/s1.

Author Contributions: S. Šegota critically analysed the data, contributed to the interpretation of the results and wrote corresponding parts of the text; G. Baranović performed the FTIR measurements, A. Sadžak and L. Mandić prepared MSNs and performed the UV-Vis measurements; A. Sadžak, V. Strasser and S. Šegota performed AFM measurements V. Strasser, D. Domazet Jurašin, and M. Dutour Sikirić performed the DLS, UV/VIS and zeta-potential measurements.

Funding: This work has been fully supported by Croatian Science Foundation under the project IP-2016-06-8415 and by Croatian Agency for SMEs, Innovations and Investments under the project PoC6_11_46.

Acknowledgments: The authors thank dr. sc. Jasminka Popović and Elizabeta Stojaković for their help in discussion, experimental planning and performing the experiments.

Conflicts of Interest: The authors declare no conflict of interest.

Abbreviations

d_H	hydrodynamic diameter
DLS	dynamic light scattering
DOPC	1,2-dioleoyl-sn-glycero-3-phosphocholine
ELS	electrophoretic light scattering
LE	Loading efficiency
MLV	multilamellar vesicles
MSNs	mesoporous silica nanoparticles
NPs	nanoparticles
PBS	phosphate buffer solution
SLB	

References

1. Federico, A.; Cardaioli, E.; Da Pozzo, P.; Formichi, P.; Gallus, G. N.; Radi, E. Mitochondria, oxidative stress and neurodegeneration. *J. Neurol. Sci*. **2012**, *322*, 2542-2562. (doi: 10.1016/j.jns.2012.05.030).
2. Ossola, B.; Kääriäinen, T. M.; Männistö, P. T. The multiple faces of quercetin in neuroprotection. *Expert. Opin. Drug Saf*. **2009**, *8*, 397–409. (doi: 10.1517/14740330903026944).
3. Slemmer, J. E.; Shacka, J.J.; Sweeney, M.I.; Weber, J.T. Antioxidants and free radical scavengers for the treatment of stroke, traumatic brain injury and aging. *Curr. Med. Chem.* **2008**, *15*, 404-414. (doi: 10.2174/092986708783497337).
4. Kelsey, N.A.; Wilkins, H.M.; Linseman, D.I.A. Nutraceutical Antioxidants as Novel Neuroprotective Agents. *Molecules* **2010**, *15*, 7779-7814. (doi: 10.3390/molecules15117792)
5. Martins, I.L.; Charneira, C.; Gandin, V.; Ferreira da Silva, J.L.; Justino, G.C.; Telo, J.P.; Vieira, A.J.; Marzano, C.; Antunes, A.M. Selenium-containing chrysin and quercetin derivatives: attractive scaffolds for cancer therapy. *Mdic. Chem*. **2015**, *58*, 4250–4265. (doi: 10.1021/acs.jmedchem.5b00230)
6. Li, M.M.; Su, X. Q.; Sun, J.; Gu, Y.F.; Huang, Z.; Zeng, K.W. Anti-inflammatory ursane- and oleanane-type triterpenoids from Vitex negundo var. cannabifolia. *J.Natural Produc*. **2014,** *77*, 2248–2254. (doi: 10.1021/np500509q)
7. Hendra, R.; Ahmad, S.; Sukari, A.; Shukor, M.Y.; Oskoueian, E. Flavonoid Analyses and Antimicrobial Activity of Various Parts of Phaleria macrocarpa (Scheff.) Boerl Fruit. *Int. J. Mol. Sci.* **2011**, *12*, 3422–3431. (doi: 10.3390/ijms12063422)
8. Baptista, F.I.; Henriques, A.G.; Silva, A.M.S.; Wiltfang, J.; da Cruz e Silva, O.A.B. Flavonoids as Therapeutic Compounds Targeting Key Proteins Involved in Alzheimer's Disease. *ACS Chem. Neurosci.* **2014**, *5*, 83–92. (doi: 10.1021/cn400213r)

9. Chu, D.; Tian, J.; Liu, W.; Li, Z.; Li, Y. Poly(Lactic-co-glycolic Acid) Microspheres for the Controlled Release of Huperzine A: In Vitro and in Vivo Studies and the Application in the Treatment of the Impaired Memory of Mice. *Chem. Pharm. Bull. (Tokyo).* **2007**, *55*, 625–628. (doi: 10.1248/cpb.55.625)

10. Pool, H.; Quintanar, D.; Figueroa, J. de D.; Marinho Mano, C.; Bechara, J.E.H.; Godínez, L.A.; Mendoza, S. Antioxidant Effects of Quercetin and Catechin Encapsulated into PLGA Nanoparticles. *J. Nanomater.* **2012**, *2012*, 1–12. (doi: 10.1155/2012/145380)
11. Baeza, A.; Colilla, M.; Vallet-Regí, M. Advances in mesoporous silica nanoparticles for targeted stimuli-responsive drug delivery. *Expert Opin. Drug Deliv.* **2015**, *12*, 319–337. (doi: 10.1517/17425247.2014.953051)
12. Wang, Y.; Zhao, Q.; Han, N.; Bai, L.; Li, J.; Liu, J.; Che, E.; Hu, L.; Zhang, Q.; Jiang, T.; et al. Mesoporous silica nanoparticles in drug delivery and biomedical applications. *Nanomedicine Nanotechnology, Biol. Med.* **2015**, *11*, 313–327. (doi: 10.1016/j.nano.2014.09.014)
13. Kierys, A.; Rawski, M.; Goworek, J. Polymer–silica composite as a carrier of an active pharmaceutical ingredient. *Microporous Mesoporous Mater.* **2014**, *193*, 40–46. (doi: 10.1016/j.micromeso.2014.03.011)
14. Mahapatro, A.; Singh, D.K. Biodegradable nanoparticles are excellent vehicle for site directed in-vivo delivery of drugs and vaccines. J. Nanobiotechnology 2011, 55, 1-11. (doi: 10.1186/1477-3155-9-55)
15. Gupta, P.; Authimoolam, S.P.; Hilt, J.Z.; Dziubla, T.D. Quercetin conjugated poly(β-amino esters) nanogels for the treatment of cellular oxidative stress. *Acta Biomater.* **2015**, *27*, 194–204. (doi: 10.1016/j.actbio.2015.08.039)
16. Shen, S.; Wu, Y.; Liu, Y.; Wu, D. High drug-loading nanomedicines: progress, current status, and prospects. *Int. J. Nanomedicine.* **2017,** *31*, 4085-4109. (doi: 10.2147/IJN.S132780)
17. Das, D.K.; Chakraborty, A.; Bhattacharjee, S.; Dey, S. Biosynthesis of stabilised gold nanoparticle using an aglycone flavonoid, quercetin. *J. Exp. Nanosci.* **2013**, *8*, 649–655. (doi: 10.1080/17458080.2011.591001)
18. Kumar, B.; Smita, K.; Cumbal, L.; Debut, A.; Angulo, Y. Biofabrication of copper oxide nanoparticles using Andean blackberry (Rubus glaucus Benth.) fruit and leaf. *J. Saudi Chem. Soc.* **2017**, *21*, S475–S480. (doi: 10.1016/j.jscs.2015.01.009)
19. Kurepa, J.; Nakabayashi, R.; Paunesku, T.; Suzuki, M.; Saito, K.; Woloschak, G.E.; Smalle, J.A. Direct isolation of flavonoids from plants using ultra-small anatase TiO 2 nanoparticles. *Plant J.* **2014**, *77*, 443–453. (doi: 10.1111/tpj.12361)
20. Bennet, D.; Kim, S. Polymer Nanoparticles for Smart Drug Delivery. In *Application of Nanotechnology in Drug Delivery*; InTech, 2014.
21. Sapino, S.; Ugazio, E.; Gastaldi, L.; Miletto, I.; Berlier, G.; Zonari, D.; Oliaro-BossoS. Mesoporous silica as topical nanocarriers for quercetin: characterization and in vitro studies, Eur. J. Pharm. Biopharm. 2015, 89, 116-125. (doi: 10.1016/j.ejpb.2014.11.022)
22. AbouAitah, K. E.A.; Farghali, A. A.; Swiderska-Sroda, A.; Lojkowski, W.; Razin, A.F. M.; Khedr, M. H., Mesoporous Silica Materials in Drug Delivery System: pH/Glutathione- Responsive Release of Poorly Water-Soluble Pro-drug Quercetin from Two and Three-dimensional Pore-Structure Nanoparticles, J. Nanomed. Nanotechnol. 2016, 7, 2-12. (doi: 10.4172/2157-7439.1000360)
23. Huang, X.; Young, N.P.; Townley, H.E. Characterization and Comparison of Mesoporous Silica Particles for Optimized Drug Delivery. *Nanomater. Nanotechnol.* **2014**, *4*, 1-15. (doi: 10.5772/58290)
24. Dave, P.N.; Chopda, L. V. A Review on Application of Multifunctional Mesoporous Nanoparticles in Controlled Release of Drug Delivery. *Mater. Sci. Forum* **2014**, *781*, 17–24. (doi: 10.4028/www.scientific.net/MSF.781.17)
25. Han, N.; Wang, Y.; Bai, J.; Liu, J.; Wang, Y.; Gao, Y.; Jiang, T.; Kang, W.; Wang, S. Facile synthesis of the lipid bilayer coated mesoporous silica nanocomposites and their application in drug delivery. *Microporous Mesoporous Mater.* **2016**, *219*, 209–218. (doi:10.1016/j.micromeso.2015.08.006)
26. Nday, C. M.: Halevas, E.; Jackson, G. E.; Salifoglou, A. Quercetin encapsulation in modified silica nanoparticles: potential use against Cu(II)-induced oxidative stress in neurodegeneration. J. Inorg. Biochem. 2015,145,51-6. (doi: 10.1016/j.jinorgbio.2015.01.001)
27. Jazvinšćak Jembrek, M.; Vuković, L.; Puhović, J.; Erhardt, J.; Oršolić, N. Neuroprotective Effect of Quercetin Against Hydrogen Peroxide-induced Oxidative Injury in P19 Neurons. *J. Mol. Neurosci.* **2012**, *47*, 286–299. (doi: 10.1007/s12031-012-9737-1)

28. Jazvinšćak Jembrek, M.; Vlainić, J.; Čadež, V.; Šegota, S. Atomic force microscopy reveals new biophysical markers for monitoring subcellular changes in oxidative injury: Neuroprotective effects of quercetin at the nanoscale. *PLoS One* **2018**, *13*, e0200119. (doi: 10.1371/journal.pone.0200119)
29. Choi, S.-M.; Kim, B.C.; Cho, Y.-H.; Choi, K.-H.; Chang, J.; Park, M.-S.; Kim, M.-K.; Cho, K.-H.; Kim, J.-K. Effects of Flavonoid Compounds on β-amyloid-peptide-induced Neuronal Death in Cultured Mouse Cortical Neurons. *Chonnam Med. J.* **2014**, *50*, 45-51. (doi: 10.4068/cmj.2014.50.2.45)
30. Domitrović, R.; Rashed, K.; Cvijanović, O.; Vladimir-Knežević, S.; Škoda, M.; Višnić, A. Myricitrin exhibits antioxidant, anti-inflammatory and antifibrotic activity in carbon tetrachloride-intoxicated mice. *Chem. Biol. Interact.* **2015**, *230*, 21–29. (doi: 10.1016/j.cbi.2015.01.030)
31. Knekt, P.; Kumpulainen, J.; Järvinen, R.; Rissanen, H.; Heliövaara, M.; Reunanen, A.; Hakulinen, T.; Aromaa, A. Flavonoid intake and risk of chronic diseases. *Am. J. Clin. Nutr.* **2002**, *76*, 560–568. (doi: 10.1093/ajcn/76.3.560)
32. Shimosaki, S.; Tsurunaga, Y.; Itamura, H.; Nakamura, M. Anti-allergic effect of the flavonoid myricitrin from Myrica rubra leaf extracts in vitro and in vivo. *Nat. Prod. Res.* **2011**, *25*, 374–380. (doi: 10.1080/14786411003774320)
33. Meotti, F.C. Analysis of the Antinociceptive Effect of the Flavonoid Myricitrin: Evidence for a Role of the L-Arginine-Nitric Oxide and Protein Kinase C Pathways. *J. Pharmacol. Exp. Ther.* **2005**, *316*, 789–796. (doi: 10.1124/jpet.105.092825)
34. Šegota S.; Vojta D.; Pletikapić G.; Baranović G. Ionic strength and composition govern the elasticity of biological membranes. *Chem. Phys. Lipids* **2015**, *186*, 17-29. (doi: 10.1016/j.chemphyslip.2014.11.001)
35. Šegota S.; Vojta D.; Kendziora D.; Ahmed I.; Fruk Lj.; Baranović G. Ligand-Dependent Nanoparticle Clustering within Lipid Membranes Induced by Surrounding Medium. *J. Phys. Chem. B.* **2015**, *119*, 5208-5219. (doi: 10.1021/acs.jpcb.7b00500)
36. Margina D.; Ilie M.; Manda G.; Neagoe I.; Mocanu M.; Ionescu D.; Gradinaru D.; Ganea G. Quercetin and epigallocatechin gallate effects on the cell membranes biophysical properties correlate with their antioxidant potential. *Gen. Physiol. Biophys.* **2012**, *31*, 47–55. (doi: 10.4149/gpb_2012_005)
37. Pawlikowska-Pawlęga B., Dziubińska H.; Król E.; Trębacz K.; Jarosz-Wilkołazka A.; Paduch R.; Gawron A.; Gruszecki W. I. Characteristics of quercetin interactions with liposomal and vacuolar membranes. *Biochim Biophys Acta* **2014**, *1838*, 254–265.(doi: 10.1016/j.bbamem.2013.08.014)
38. Londoño-Londoño J.; De Lima V. R.; Jaramillo C.; Creczynski-pasa T. Hesperidin and hesperetin membrane interaction: Understanding the role of 7-O-glycoside moiety in flavonoids. *Arch Biochem Biophys* **2010**, *499*, 6–16. (doi: 10.1016/j.abb.2010.04.023)
39. Arczewska M.; Kamiński D. M., Górecka E.; Pociecha D.; Rój E.; Sławińska-Brych A.; Gagoś M. The molecular organization of prenylated flavonoid xanthohumol in DPPC multibilayers: X-ray diffraction and FTIR spectroscopic studies. *Biochim Biophys Acta* **2013**, *1828*, 213–222. (doi: 10.1016/j.bbamem.2012.10.009)
40. Freudenthal O.; Quilès F.; Francius G.; Wojszko K.; Gorczyc M., Korchowiec B.; Rogalska E. Nanoscale investigation of the interaction of colistin with model phospholipid membranes by Langmuir technique, and combined infrared and force spectroscopies. *Biochim Biophys Acta* **2016,** *1858*, 2592–2602. (doi10.1016/j.bbamem.2016.07.015:)
41. Selvaraj S.; Krishnaswamy S.; Devashya V.; Sethuraman S.; Krishnan, U.M. Influence of membrane lipid composition on flavonoid-membrane interactions: Implications on their biological activity. *Prog. Lipid Res.* **2015**, *58*, 1–13. (doi: 10.1016/j.plipres.2014.11.002)
42. Attwood S. J.; Choi Y.; Leonenko Z. Preparation of DOPC and DPPC Supported Planar Lipid Bilayers for Atomic Force Microscopy and Atomic Force Spectroscopy. *Int. J. Mol. Sci.* **2013**, *14*, 3514-3539. (doi:10.3390/ijms14023514.)
43. Jazvinšćak Jembrek M.; Simic G.; Hof P.; Šegota S., Atomic force microscopy as an advanced tool in neuroscience. *Transl Neurosci.* **2015**, *6*, 117–130. (doi: 10.1515/tnsci-2015-0011)
44. Ollila F.; Halling K.; Vuorela P.; Vuorela H.; Slotte J. P., Characterization of Flavonoid–Biomembrane Interactions. *Arch. Biochem. Biophys.* **2002**, *399*, 103–108. (doi: 10.1006/abbi.2001.2759)
45. Tushiya H., Membrane Interactions of Phytochemicals as Their Molecular Mechanism Applicable to the Discovery of Drug Leads from Plants. *Molecules* **2015**, *20*, 18923-18966. (doi: 10.3390/molecules201018923)

46. Arora A.; Byrem T. M.; Nair M. G.; Strasburg G.M., Modulation of liposomal membrane fluidity by flavonoids and isoflavonoids. *Arch. Biochem*. Biophys. **2000**, *373*, 102–109. (doi: 10.1006/abbi.1999.1525)
47. Soto-Cantu E.; Cueto R.; Koch J.; Russo P. S., Synthesis and Rapid Characterization of Amine-Functionalized Silica, *Langmuir* **2012**, *28*, 5562−5569. (doi: 10.1021/la204981b)
48. Li Y.; Qi X.R.; Maitani Y.; Nagai T., PEG-PLA diblock copolymer micelle-like nanoparticles as all-trans-retinoic acid carrier: in vitro and in vivo characterizations. *Nanotechnology* **2009,** 20(5). (doi: 10.1088/0957-4484/20/5/055106)
49. Rio-Echevarria I. M.; Selvestrel F.; Segat D.; Guarino G.; Tavano R.; Causin V.; Reddi E.; Papini E.; Mancin F., Highly PEGylated silica nanoparticles: "ready to use" stealth functional nanocarriers. *J. Mater. Chem.* **2010**, *20,* 2780-2787. (doi: 10.1039/B921735E)
50. Allen T. M.; Hansen C.; Martin F.; Redemann C.; Yau-Young A., Liposomes containing synthetic lipid derivatives of poly(ethylene glycol) show prolonged circulation half-lives in vivo. *Biochim. Biophys. Acta.* **1991,** *1066*, 29–36. (doi: 10.1016/0005-2736(91)90246-5)
51. Lasic D. D.; Woodle M. C.; Martin F. J.; Valentincic T., Phase behavior of "stealth-lipid"-lecithin mixtures. *Period. Biol.* **1991**, *93*, 287-290. (doi: 10.1016/S0006-3495(03)74798-5)
52. Jeon S. I.; Lee J.H., Andrade J. D.; De Gennes P.G. Protein—surface interactions in the presence of polyethylene oxide: I. Simplified theory. *J Colloid Interface Sci.* **1991,** *142*, 149–158. (doi: 10.1016/0021-9797(91)90043-8)
53. Catauro M.; Papale F.; Bollino F.; Piccolella S.; Marciano S.; Nocera P.; Pacifico S. Silica/quercetin sol–gel hybrids as antioxidant dental implant materials. *Sci. Technol. Adv. Mater.* **2015,** *16*, 035001-035012.(doi: 10.1088/1468-6996/16/3/035001)
54. Li Y.; Jao J.; Han C.;Yang J.; Tabassum Chaudhry M.; Wang S.; Liu H.; Yin Y. Quercetin, Inflammation and Immunity. *Nutrients* **2016,** *8*, 167-181. (doi: 10.3390/nu8030167)
55. Franklin S. J.; Myrdal P. B. Solid-State and Solution Characterization of Myricetin, AAPS. Pharm. Sci. Tech. 2015, 16,1400–1408. (doi: 10.1208/s12249-015-0329-6)
56. https://comptox.epa.gov/dashboard/dsstoxdb/results?search=DCYOADKBABEMIQ#toxval (accessed 14.04. 2018).
57. Maity P.; Saha B.; Suresh Kumar G.; Karmakar S. Binding of monovalent alkali metal ions with negatively chargedphospholipid membranes. *Biochim. Biophys. Acta.* **2016**, *1858*, 706–714. (doi: 10.1016/j.bbamem.2016.01.012)
58. Harris C. S.; Mo F.; Migahed L.; Chepelev L.; Haddad P. S.; Wright J. S.; Willmore W. G; Arnason J. T.; Bennett S. A .L. Plant phenolics regulate neoplastic cell growth and survival: a quantitative structure–activity and biochemical analysis. *Can. J. Physiol. Pharmacol***. 2007,** *85*, 1124-1138. (doi**:** 10.1139/Y07-101)
59. Alvarez-Diduk R.; Ramirez-Silva M. T.; Galano A.; Merkoci A. Deprotonation mechanism and acidity constants in aqueous solution of flavonols. A combined experimental and theoretical study. *J. Phys. Chem. B* **2013**, *117*, 12347-12359. (doi: 10.1021/jp4049617)
60. Bi S.; Wang T.; Zhao T.; Wang Yu; Pang B. Study of the interaction of salmon sperm DNA with myricitrin–CPB based on the enhanced resonance light scattering signal and its potential application, Spectrochimica Acta Part A: Molecular and Biomolecular *Spectroscopy* **2013**, *112*, 397–402. (doi: 10.1016/j.saa.2012.01.037)
61. Engel A.; Schoenenberger C.-A.; Muller D. J. High Resolution Imaging of Native Biological Sample Surfaces Using Scanning Probe Microscopy. *Curr. Opin. Struct. Biol.* **1997**, *7*, 279–284. (doi: 10.1038/nprot.2007.309)
62. Santoro A. L.; Carrilho E.; Lancas F. M.; Montanari C. A., Quantitative structure–retention relationships of flavonoids unraveled by immobilized artificial membrane chromatography. *Eur. J. Pharm. Sci.* **2016**, *88*, 147-157. (doi: 10.1016/j.ejps.2015.12.009)
63. Serra H.; Mendes T.; Bronze M. R.; Simplicio A. L., Prediction of intestinal absorption and metabolism of pharmacologically active flavones and flavanones. *Bioorg. Med. Chem.* **2008**, *16*, 4009–4018. (doi: 110.1016/j.bmc.2008.01.028)
64. Roa J. J; Oncins G.; Diaz J.; Sanz F.; Segarra M. Calculation of Young's modulus value by means of AFM, *Recent Pat Nanotechnol.* **2011**, *5*, 27-36. (doi: 10.2174/187221011794474985)